



HAL
open science

Quantum centipedes: collective dynamics of interacting quantum walkers

P. L. Krapivsky, J. M. Luck, Kirone Mallick

► **To cite this version:**

P. L. Krapivsky, J. M. Luck, Kirone Mallick. Quantum centipedes: collective dynamics of interacting quantum walkers. *Journal of Physics A: Mathematical and Theoretical*, 2016, 49, pp.335303. 10.1088/1751-8113/49/33/335303 . cea-01307044

HAL Id: cea-01307044

<https://cea.hal.science/cea-01307044>

Submitted on 23 Oct 2020

HAL is a multi-disciplinary open access archive for the deposit and dissemination of scientific research documents, whether they are published or not. The documents may come from teaching and research institutions in France or abroad, or from public or private research centers.

L'archive ouverte pluridisciplinaire **HAL**, est destinée au dépôt et à la diffusion de documents scientifiques de niveau recherche, publiés ou non, émanant des établissements d'enseignement et de recherche français ou étrangers, des laboratoires publics ou privés.

Quantum centipedes: collective dynamics of interacting quantum walkers

P L Krapivsky^{1,2}, J M Luck² and K Mallick²

¹ Department of Physics, Boston University, Boston, MA 02215, USA

² Institut de Physique Théorique, Université Paris-Saclay, CEA and CNRS, 91191 Gif-sur-Yvette, France

Abstract. We consider the quantum centipede made of N fermionic quantum walkers on the one-dimensional lattice interacting by means of the simplest of all hard-bound constraints: the distance between two consecutive fermions is either one or two lattice spacings. This composite quantum walker spreads ballistically, just as the simple quantum walk. However, because of the interactions between the internal degrees of freedom, the distribution of its center-of-mass velocity displays numerous ballistic fronts in the long-time limit, corresponding to singularities in the empirical velocity distribution. The spectrum of the centipede and the corresponding group velocities are analyzed by direct means for the first few values of N . Some analytical results are obtained for arbitrary N by exploiting an exact mapping of the problem onto a free-fermion system. We thus derive the maximal velocity describing the ballistic spreading of the two extremal fronts of the centipede wavefunction, including its non-trivial value in the large- N limit.

E-mail: pkrapivsky@gmail.com, jean-marc.luck@cea.fr, kirone.mallick@cea.fr

1. Introduction

Quantum walks [1], the quantum analogues of classical random walks, play a prominent role in quantum information theory [2]. It has been shown in [3] that any quantum algorithm can be restated in terms of quantum walks. These universal objects are the source of fascinating problems mixing wave dynamics, discrete geometry and probability theory. Quantum dynamics often results in a counter-intuitive phenomenology: quantities like hitting times or survival probabilities of a walker are genuinely different in quantum and classical set-ups; in particular, a quantum search can be far more efficient than a classical algorithm (see e.g. [4, 5, 6] for reviews).

Single-particle quantum walks have been realized in the laboratory, using nuclear magnetic resonance [7], trapped ions or atoms [8, 9, 10] and photons [11]. The behavior of a single quantum walker can be explained by a wave description [12] and reproduced in an experiment with classical waves [13].

Non-classical effects become essential if one considers multiple quantum walkers. Quantum walks of correlated photons have been implemented experimentally by various groups [14, 15, 16, 17]. In such systems, quantum interferences and interactions lead to entanglement and correlations that can not be accounted for by a classical picture, triggering thus much interest among theorists [18, 19, 20, 21, 22].

A single quantum walker displays a ballistic rather than a diffusive motion. It spreads over a range of space that grows linearly with time. Surprisingly, the wavefunction displays sharp maxima near the boundaries of that allowed range, whereas it is negligibly small beyond this range. These maxima can be interpreted as ballistic fronts [2, 23]. In a recent work [24], we have investigated the dynamics of bosonic and fermionic bound states of two interacting continuous-time quantum walkers in one dimension. The emphasis was on the ballistic spreading of the center-of-mass coordinate. We have demonstrated the existence of multiple internal ballistic fronts, corresponding to singularities of the velocity distribution, besides the two usual extremal ones. This feature is robust and generic, regardless of the statistics and of the precise form of the interaction potential between the two particles.

The aim of the present work is to investigate the center-of-mass dynamics, and especially the ballistic fronts, displayed by a composite object made of N fermionic quantum walkers on a one-dimensional lattice, constrained to remain within a fixed distance ℓ from their neighbors. This problem can be viewed as quantum-mechanical version of the diffusive dynamics of the N -legged molecular spiders that were considered in [25], hence the name *quantum centipede*. In this work we focus our attention onto the simplest of all centipedes, corresponding to $\ell = 2$. In this special situation, some analytical results can be derived by exploiting an exact mapping of the problem onto a free-fermion system.

The outline of this paper is as follows. In section 2 we review known results on one-dimensional continuous-time quantum walks, both for a single walker and for a pair of interacting walkers. The fermionic quantum centipede studied in this work is defined in section 3. In section 4 we map the problem onto an integrable XX Heisenberg spin chain, which can be reduced to a free-fermion system and diagonalized by means of a Jordan-Wigner transformation. Explicit results on the spectrum of the quantum centipede are presented in section 5 for the first few values of the fermion number ($N = 2$ to 5). In section 6 we obtain the maximal spreading velocities $V^{(N)}$ for arbitrary N , as well as their limit $V^{(\infty)}$. Section 7 contains a discussion of our findings. A derivation of the characteristic equations (4.14), (4.15) is given in Appendix A.

2. A summary of earlier results on one and two quantum walkers

We consider continuous-time quantum walks on the discrete one-dimensional lattice. There is no need for an internal degree of freedom (quantum coin), as would be required for discrete-time dynamics. We recall some elementary results for the single quantum walk [2, 4, 5, 6, 23], and then discuss the case of two co-walking particles, with an emphasis on the ballistic fronts (see [24] and the references therein).

2.1. The simple quantum walker

The simple continuous-time quantum walk is modeled by a tight-binding Hamiltonian, in which the walker hops from a site to a neighboring site. We denote by $\psi_n(t) = \langle n | \psi(t) \rangle$ the wavefunction of the particle at site n at time t , and use dimensionless units. The dynamics of the walker is given by

$$i \frac{d\psi_n(t)}{dt} = \psi_{n+1}(t) + \psi_{n-1}(t). \quad (2.1)$$

Suppose that the particle is launched from the origin at time $t = 0$: $\psi_n(0) = \delta_{n0}$. The wavefunction at time t is then given by a Bessel function:

$$\psi_n(t) = i^{-n} J_n(2t). \quad (2.2)$$

Asymptotic properties of Bessel functions allow us to analyze the spreading of the quantum walk in the long-time limit [23]. The asymptotic probability distribution of the effective velocity $v = n/t$ has a compact support and converges to an ‘arc-sine law’:

$$f(v) = \frac{1}{\pi\sqrt{4-v^2}} \quad (|v| < 2). \quad (2.3)$$

We emphasize that, in contrast to the classical case, the convergence is in the weak sense: the probability distribution $|\psi_n(t)|^2$ displays high-frequency oscillations which must be averaged out to derive the function $f(v)$ [26, 27, 28, 29, 30].

At late times, the quantum particle is therefore almost surely located in the allowed region ($|n| < 2t$). A more precise analysis shows that the probabilities $|\psi_n(t)|^2$ display sharp ballistic fronts near the endpoints of the allowed region ($n = \pm 2t$), with a height scaling as $t^{-2/3}$ and a width scaling as $t^{1/3}$. The above generic behavior remains unchanged as long as the initial state is localized in a finite region: the quantum walker spreads ballistically in the allowed region limited by ballistic fronts near $n = \pm 2t$, with a forbidden region beyond them. It is however possible to engineer exceptional initial states, for which either one or even both fronts are eliminated by quantum interferences [24], but these features are non-generic.

The picture changes qualitatively if the particle is allowed to hop to the next-nearest neighboring sites with a transition amplitude g :

$$i \frac{d\psi_n(t)}{dt} = \psi_{n+1}(t) + \psi_{n-1}(t) + g(\psi_{n+2}(t) + \psi_{n-2}(t)). \quad (2.4)$$

Allowing hopping to second and further neighbors is known to have far reaching consequences in a variety of situations [31, 32, 33, 34]. For instance, in the case of graphene [35, 36], hopping to second neighbors breaks the chiral symmetry between both sublattices. In the present case, when $g > 1/4$, the probability distribution of the velocity $v = n/t$ becomes singular at four values. The quantum walker thus exhibits four fronts: two external fronts (as above) at $v = \pm V_+$, and also two internal fronts at $v = \pm V_-$ [24]. If longer range hopping is allowed and if the corresponding hopping amplitudes exceed critical values, more internal fronts might appear for generic initial conditions.

2.2. Two co-walking quantum particles

The continuous-time quantum walk problem can be generalized by considering several interacting quantum walkers. In a recent work [24], we have investigated the quantum walk performed by two identical particles interacting either through hard-bound constraints or by a smooth confining potential. The statistics of the particles (bosonic or fermionic) turned out to play an important role in the analysis of the ballistic spreading of the bound states thus obtained.

We briefly summarize the results of [24] for the quantum walk of two one-dimensional fermions interacting by the hard-bound constraint that their distance is at most ℓ lattice spacings. We denote by $n_1 = n + m$ and $n_2 = n$ the positions of the particles, so that $n_{\text{cm}} = n + m/2$ is the center-of-mass coordinate, whereas $m = n_1 - n_2$ is the relative coordinate. The hard-bound constraint imposes that $|m| \leq \ell$. This fermionic system is described by the wavefunction

$$\psi_{n,m}(t) = \langle (n_1, n_2) | \psi(t) \rangle = \langle (n + m, n) | \psi(t) \rangle, \quad (2.5)$$

which is odd with respect to m . Because fermionic particles can not cross one another in one dimension, m can be restricted to the range $m = 1, \dots, \ell$. The dynamics is then given by

$$i \frac{d\psi_{n,m}(t)}{dt} = \psi_{n,m-1}(t) + \psi_{n+1,m-1}(t) + \psi_{n-1,m+1}(t) + \psi_{n,m+1}(t), \quad (2.6)$$

with Dirichlet boundary conditions: $\psi_{n,0}(t) = \psi_{n,\ell+1}(t) = 0$.

The exact solution of this two-body problem displays the following features. The wavefunction again spreads ballistically in the center-of-mass coordinate. For late times, the components $\psi_{n,m}(t)$ of the wavefunction have appreciable values for a range of n that grows ballistically and symmetrically with respect to the origin. The probability distribution $|\psi_{n,m}(t)|^2$ of the bound state in its center-of-mass coordinate generically exhibits sharp ballistic fronts for $n \approx V_k t$, where the front velocities read

$$V_k = 2 \cos \frac{k\pi}{\ell+1} \quad (k = 1, \dots, \ell). \quad (2.7)$$

The spreading dynamics is therefore characterized by two extremal fronts, and $\ell - 2$ internal ones for $\ell \geq 3$. The range of the allowed zone is $|n| < Vt$, the maximal spreading velocity being

$$V = 2 \cos \frac{\pi}{\ell+1}. \quad (2.8)$$

In the limit where the extent of the bound state diverges ($\ell \rightarrow \infty$), the above result approaches the free value $V = 2$, with a $1/\ell^2$ correction.

This picture remains qualitatively unchanged if the hard-bound constraint is replaced by a smooth confining potential. The bosonic and fermionic spectra are infinite sequences of dispersive energy levels, each of which giving rise to a ballistic front. These spectra have been studied in detail in the case where the confining potential is homogeneous, i.e., of the form $W_m = g|m|^\alpha$. In particular, the maximal spreading velocity of two-fermion bound states departs from its free value $V = 2$ according to

$$V \approx 2 - C^{(\text{F})} g^{2/(\alpha+3)} \quad (2.9)$$

at weak coupling ($g \ll 1$), where the constant $C^{(\text{F})}$ has been determined [24].

3. The fermionic quantum centipede

We now introduce the system we study in this work. It is the quantum centipede made of N interacting fermionic quantum walkers on the one-dimensional lattice. The interaction is modeled by the simplest of all hard-bound constraints: the distance between two consecutive fermions is either one or two lattice spacings. Besides the number N of fermions, the model is entirely parameter-free.

One-dimensional fermions cannot cross each other, and so the discrete positions of the particles along the chain can be assumed to be ordered as $x_1 < x_2 < \dots < x_N$. We label the state of the quantum centipede by the following variables:

- $n = x_1$ denotes the position of the leftmost fermion along the chain,
- the internal state of the centipede is described by a string $\varepsilon = (\varepsilon_1, \dots, \varepsilon_{N-1})$ of $N - 1$ binary variables, with $\varepsilon_j = x_{j+1} - x_j - 1 = 0$ or 1 for $j = 1, \dots, N - 1$. We have thus $\varepsilon_j = 0$ if fermions j and $j + 1$ are adjacent, while $\varepsilon_j = 1$ if they are separated by a single empty site.

Figure 1 shows a configuration of 6 fermions and the corresponding string ε .

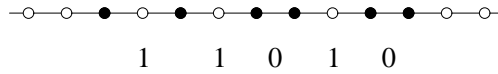


Figure 1. A configuration of 6 fermions obeying the hard-bound constraint and the corresponding string ε of 5 binary variables.

The center-of-mass coordinate of the centipede reads

$$x_{\text{cm}} = n + \frac{N-1}{2} + \frac{1}{N} \sum_{j=1}^{N-1} (N-j)\varepsilon_j. \quad (3.1)$$

We have $x_{\text{cm}} = n + (N-1)/2$ for the most compact internal state ($\varepsilon_j = 0$ for all j), whereas $x_{\text{cm}} = n + N - 1$ for the most extended one ($\varepsilon_j = 1$ for all j).

The 2^{N-1} amplitudes of N -body wavefunction

$$\psi_n^\varepsilon(t) = \langle x_1, x_2, \dots, x_N | \psi(t) \rangle \quad (3.2)$$

satisfy coupled continuous-time dynamical equations, which are analogous to (2.6). We shall not need to write down these equations explicitly, except for $N = 2$ (see (5.1)) and $N = 3$ (see (5.8)). The system is spatially homogeneous, i.e., invariant under discrete translations. It is therefore convenient to perform a Fourier transform with respect to n and define

$$\hat{\psi}^\varepsilon(q, t) = \sum_n e^{-iqn} \psi_n^\varepsilon(t), \quad (3.3)$$

where the center-of-mass momentum q can be restricted to the first Brillouin zone ($|q| \leq \pi$).

The dynamics of the amplitudes (3.3) is governed by an effective dispersive (i.e., q -dependent) Hamiltonian \mathcal{H} , represented by a Hermitian matrix of size $2^{N-1} \times 2^{N-1}$ (see e.g. (5.2), (5.9), (5.14)). The energy spectrum of the centipede therefore has 2^{N-1} branches, i.e., the eigenvalues $\omega_a(q)$ of \mathcal{H} , with $a = 1, \dots, 2^{N-1}$. The corresponding branches of the group velocity read

$$v_a(q) = \frac{d\omega_a(q)}{dq}. \quad (3.4)$$

We shall be mostly interested in the maximal velocity

$$V^{(N)} = \max_{a,q} |v_a(q)|, \quad (3.5)$$

describing the ballistic spreading of the two extremal fronts of the wavefunction in the center-of-mass coordinate, as well as in the internal ballistic fronts, characterized by all the other stationary values of the group velocity, such that

$$\frac{dv_a(q)}{dq} = \frac{d^2\omega_a(q)}{dq^2} = 0. \quad (3.6)$$

In order to proceed, we start by noticing that the action of the quantum Hamiltonian \mathcal{H} can be described in purely classical terms. The string ε is interpreted as a classical configuration of particles and holes on an open finite lattice of size $N-1$. If $\varepsilon_j = 1$, site j is occupied by a particle; if $\varepsilon_j = 0$, site j is empty. The quantum dynamics generated by \mathcal{H} corresponds to the following evolution rules:

$$\begin{aligned} \text{Bulk:} & & 10 & \rightleftharpoons & 01 & & \text{with rate } 1. \\ \text{Site 1:} & & 1 & \rightarrow & 0 & & \text{with rate } e^{-iq}, \\ & & 0 & \rightarrow & 1 & & \text{with rate } e^{iq}. \\ \text{Site } N-1: & & 1 & \rightarrow & 0 & & \text{with rate } 1, \\ & & 0 & \rightarrow & 1 & & \text{with rate } 1. \end{aligned} \quad (3.7)$$

These rules are reminiscent of the symmetric simple exclusion process (SEP) with open boundaries (see e.g. [37]). An equivalence with the SEP had already been put forward in the classical situation of the molecular spiders and centipedes investigated in [25]. There are however several notable differences between quantum-mechanical systems such as the present one and classical stochastic systems such as the SEP: (i) The quantum Hamiltonian \mathcal{H} acts on amplitudes, and not on probabilities. (ii) The transition amplitudes or ‘rates’ are not necessarily positive real numbers. (iii) The system is not equivalent to a classical stochastic process, even for $q = 0$. The Hamiltonian \mathcal{H} and the Markov operator for the SEP have the same non-diagonal elements, but the Markov operator contains diagonal loss terms, in order to ensure probability conservation, whereas the Hamiltonian \mathcal{H} does not have diagonal entries.

4. Mapping onto a free-fermion system

The energy spectrum of the quantum centipede can be determined, at least formally, by means of an exact mapping onto an integrable spin chain and finally onto a free-fermion system.

The Hamiltonian \mathcal{H} that implements the quantum dynamics (3.7) can be written, using Pauli matrices, as

$$\mathcal{H} = e^{-iq} S_1^+ + e^{iq} S_1^- + \sum_{j=1}^{N-2} (S_j^- S_{j+1}^+ + S_j^+ S_{j+1}^-) + S_{N-1}^+ + S_{N-1}^-. \quad (4.1)$$

We thus obtain the Hamiltonian of an XX spin chain with non-diagonal boundary terms [38, 39]. By convention, $\varepsilon_j = 0$ (site j is empty) corresponds to \uparrow_j (spin j is up), whereas $\varepsilon_j = 1$ (site j is occupied) corresponds to \downarrow_j (spin j is down). In the local basis $\{0_j, 1_j\} \equiv \{|\uparrow_j\rangle, |\downarrow_j\rangle\}$, the Pauli matrices are given by

$$S_j^x = \begin{pmatrix} 0 & 1 \\ 1 & 0 \end{pmatrix}, \quad S_j^y = \begin{pmatrix} 0 & -i \\ i & 0 \end{pmatrix}, \quad S_j^z = \begin{pmatrix} 1 & 0 \\ 0 & -1 \end{pmatrix} \quad (4.2)$$

and the raising and lowering operators S_j^\pm are defined as

$$S_j^+ = \frac{1}{2}(S_j^x + iS_j^y) = \begin{pmatrix} 0 & 1 \\ 0 & 0 \end{pmatrix}, \quad S_j^- = \frac{1}{2}(S_j^x - iS_j^y) = \begin{pmatrix} 0 & 0 \\ 1 & 0 \end{pmatrix}. \quad (4.3)$$

The Hamiltonian \mathcal{H} can be diagonalized by means of a Jordan-Wigner transformation [40] mapping it onto a free-fermion system. Because of the boundary terms, \mathcal{H} is not fully bilinear. This can be rectified [41, 42] by adding two auxiliary sites, one at each end of the chain, labeled 0 and N . We thus define a new Hamiltonian $\mathcal{H}_{\text{long}}$ on a chain of $N + 1$ sites as

$$\begin{aligned} \mathcal{H}_{\text{long}} = & e^{-iq} S_0^x S_1^+ + e^{iq} S_0^x S_1^- + \sum_{j=1}^{N-2} (S_j^- S_{j+1}^+ + S_j^+ S_{j+1}^-) \\ & + S_{N-1}^+ S_N^x + S_{N-1}^- S_N^x. \end{aligned} \quad (4.4)$$

The boundary operators S_0^x and S_N^x commute with $\mathcal{H}_{\text{long}}$. Hence the eigenstates of $\mathcal{H}_{\text{long}}$ belong to four distinct sectors, corresponding to the eigenvalues $(\pm 1, \pm 1)$ of the operators S_0^x and S_N^x . The restriction of $\mathcal{H}_{\text{long}}$ to the sector $(+1, +1)$ coincides with the Hamiltonian \mathcal{H} of (4.1).

The Hamiltonian $\mathcal{H}_{\text{long}}$ can be diagonalized using a fermionization procedure, as explained in [42]. The operators defined as

$$\tau_j^{x,y} = \left(\prod_{i=0}^{j-1} S_i^z \right) S_i^{x,y} \quad (j = 0, \dots, N) \quad (4.5)$$

satisfy the relations

$$\{\tau_j^\mu, \tau_k^\nu\} = 2\delta_{jk}\delta^{\mu\nu} \quad (\mu, \nu = x, y). \quad (4.6)$$

The above anti-commutation relations define a Clifford algebra. If we rewrite $\mathcal{H}_{\text{long}}$ in terms of these operators, we obtain

$$\begin{aligned} -\mathcal{H}_{\text{long}} = & i \cos q \tau_0^y \tau_1^x + i \sin q \tau_0^y \tau_1^y \\ & + \frac{i}{2} \sum_{j=1}^{N-2} (\tau_j^y \tau_{j+1}^x - \tau_j^x \tau_{j+1}^y) + i \tau_{N-1}^y \tau_N^x. \end{aligned} \quad (4.7)$$

The last step consists in expressing $\mathcal{H}_{\text{long}}$ as a free-fermion Hamiltonian:

$$\mathcal{H}_{\text{long}} = \sum_{k=0}^N \Lambda_k (2a_k^\dagger a_k - 1). \quad (4.8)$$

To do so, we must find a set of annihilation and creation operators a_k and a_k^\dagger of fermionic quasiparticles, satisfying the canonical anti-commutation relations

$$\{a_k, a_l^\dagger\} = \delta_{kl}, \quad \{a_k, a_l\} = \{a_k^\dagger, a_l^\dagger\} = 0 \quad (k = 0, \dots, N). \quad (4.9)$$

These quasiparticles are not to be confused with the original fermionic quantum walkers which constitute the centipede. The number operators $\mathcal{N}_k = a_k^\dagger a_k$ have eigenvalues 0 and 1. It follows from (4.8) that the eigenvalues of $\mathcal{H}_{\text{long}}$ are given by

$$\omega_{\text{long}} = \sum_{k=0}^N (\pm \Lambda_k), \quad (4.10)$$

where the sign \pm in front of Λ_k depends on whether the k -th quasiparticle is present ($\mathcal{N}_k = 1$) or absent ($\mathcal{N}_k = 0$).

The quasiparticle operators a_k and a_k^\dagger are obtained from the Jordan-Wigner operators $\tau_j^{x,y}$ by a Bogoliubov transformation of the form

$$\begin{aligned} a_k &= \frac{1}{2} \sum_{j=0}^N (x_{k;j} \tau_j^x + y_{k;j} \tau_j^y), \\ a_k^\dagger &= \frac{1}{2} \sum_{j=0}^N (\bar{x}_{k;j} \tau_j^x + \bar{y}_{k;j} \tau_j^y), \end{aligned} \quad (4.11)$$

where the bar denotes complex conjugation. The complex coefficients $(x_{k;j}, y_{k;j})$ are found by requiring that a_k and a_k^\dagger satisfy the canonical fermionic anti-commutation relations (4.9) and that $\mathcal{H}_{\text{long}}$ takes the diagonal form (4.8). These constraints are implemented by writing the commutation relations between $\mathcal{H}_{\text{long}}$ and a_k, a_k^\dagger :

$$[\mathcal{H}_{\text{long}}, a_k] = -2\Lambda_k a_k, \quad [\mathcal{H}_{\text{long}}, a_k^\dagger] = 2\Lambda_k a_k^\dagger. \quad (4.12)$$

Details are given in Appendix A. The quasiparticle eigenvalues are given by

$$\Lambda_k = \cos p_k, \quad (4.13)$$

where the discrete values p_k of the internal momentum p satisfy the characteristic equation (A.13), which can be further simplified by dealing separately with even and odd values of N . We obtain after some algebra

$$N \text{ even: } \sin((N+1)p) - 3 \sin((N-1)p) = \pm 4 \sin p \sin q, \quad (4.14)$$

$$N \text{ odd: } \sin((N+1)p) - 3 \sin((N-1)p) = \pm 4 \sin p \cos q. \quad (4.15)$$

5. Explicit results for the first few values of N

In this section we present explicit results for the first few values of the fermion number ($N = 2$ to 5).

- $N = 2$

This is a special case of the more general two-body problem considered in [24], where the maximal distance between the two quantum walkers is an arbitrary integer ℓ .

With the notation (3.2), the amplitudes ψ_n^0 and ψ_n^1 obey the equations

$$\begin{aligned} i \frac{d\psi_n^0(t)}{dt} &= \psi_{n-1}^1(t) + \psi_n^1(t), \\ i \frac{d\psi_n^1(t)}{dt} &= \psi_n^0(t) + \psi_{n+1}^0(t), \end{aligned} \quad (5.1)$$

which can be viewed as a special case of (2.6). The corresponding Hamiltonian reads

$$\mathcal{H} = \begin{pmatrix} 0 & 1 + e^{iq} \\ 1 + e^{-iq} & 0 \end{pmatrix}. \quad (5.2)$$

We thus readily obtain

$$\omega_{1,2} = \pm 2 \cos \frac{q}{2}. \quad (5.3)$$

The associated group velocities read

$$v_{1,2} = \mp \sin \frac{q}{2}. \quad (5.4)$$

In particular, the maximal velocities $\pm V^{(2)}$, with

$$V^{(2)} = 1, \quad (5.5)$$

are reached for $q = \pm\pi$. There is no other stationary value of the group velocity, and consequently no internal front besides the extremal ones, in agreement with the findings of [24] for $\ell = 2$, recalled in section 2.2. Figure 2 shows plots of the energy spectrum (left) and of the group velocities (right) against q/π in the first Brillouin zone.

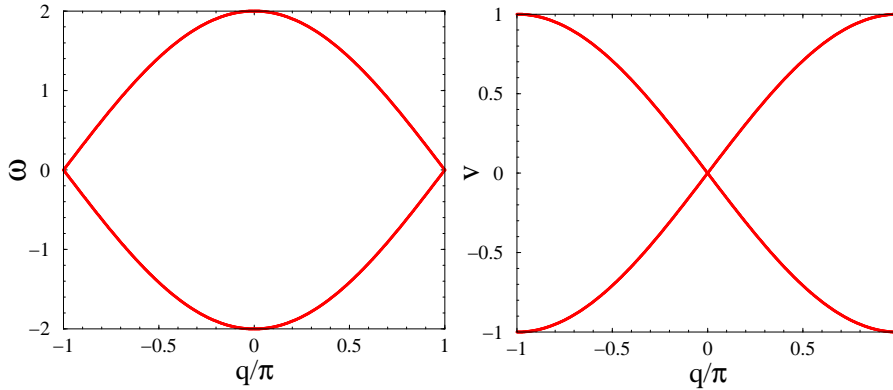


Figure 2. Left: energy spectrum of the $N = 2$ centipede against q/π . Right: associated group velocities.

Equation (4.14) yields the quasiparticle eigenvalues

$$\Lambda_{1,2} = \sqrt{1 \pm \sin q}. \quad (5.6)$$

Figure 3 shows the quasiparticle spectrum against q/π . The correspondence (4.10) relies on the following identities:

$$\omega_1 = -\omega_2 = \begin{cases} \Lambda_2 - \Lambda_1 & (-\pi \leq q \leq -\pi/2), \\ \Lambda_1 + \Lambda_2 & (-\pi/2 \leq q \leq \pi/2), \\ \Lambda_1 - \Lambda_2 & (\pi/2 \leq q \leq \pi). \end{cases} \quad (5.7)$$

- $N = 3$

The wavefunction amplitudes obey the equations

$$\begin{aligned} i \frac{d\psi_n^{00}(t)}{dt} &= \psi_{n-1}^{10}(t) + \psi_n^{01}(t), \\ i \frac{d\psi_n^{01}(t)}{dt} &= \psi_{n-1}^{11}(t) + \psi_n^{00}(t) + \psi_n^{10}(t), \\ i \frac{d\psi_n^{10}(t)}{dt} &= \psi_n^{01}(t) + \psi_n^{11}(t) + \psi_{n+1}^{00}(t), \\ i \frac{d\psi_n^{11}(t)}{dt} &= \psi_n^{10}(t) + \psi_{n+1}^{01}(t). \end{aligned} \quad (5.8)$$

The corresponding Hamiltonian reads

$$\mathcal{H} = \begin{pmatrix} 0 & 1 & e^{iq} & 0 \\ 1 & 0 & 1 & e^{iq} \\ e^{-iq} & 1 & 0 & 1 \\ 0 & e^{-iq} & 1 & 0 \end{pmatrix}. \quad (5.9)$$

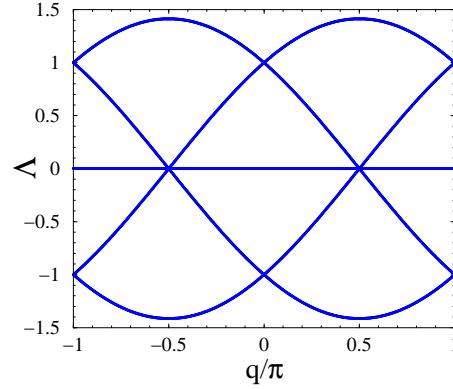


Figure 3. Quasiparticle spectrum of the $N = 2$ centipede against q/π .

The associated characteristic equation is

$$\omega(\omega^3 - 5\omega - 4 \cos q) = 0. \quad (5.10)$$

Figure 4 shows plots of the energy spectrum (left) and of the group velocities (right) against q/π . The maximal velocities $\pm V^{(3)}$, with

$$V^{(3)} = \frac{4}{5}, \quad (5.11)$$

are respectively reached for $q = \pm\pi/2$. The group velocity also exhibits a flat (i.e., non-dispersive) band, as well as four non-trivial stationary points obeying (3.6). Differentiating twice the characteristic equation (5.10), we obtain after some algebra the stationary velocities $\pm V^{(3,1)}$, with

$$V^{(3,1)} = \frac{\sqrt{5 - 17^{1/3}}}{3} = 0.519478\dots \quad (5.12)$$

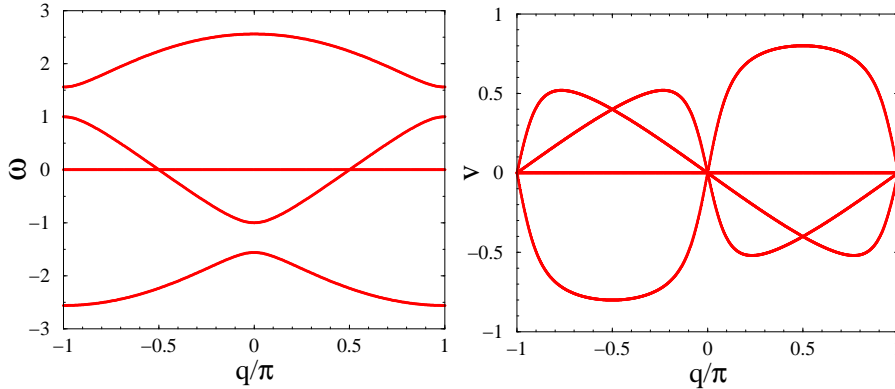


Figure 4. Left: energy spectrum of the $N = 3$ centipede against q/π . Right: associated group velocities.

These results show that the wavefunction of the 3-fermion centipede generically exhibit five ballistic peaks in the center-of-mass coordinate: two extremal ones at

$n \approx \pm V^{(3)}t$, two internal ones at $n \approx \pm V^{(3,1)}t$, and possibly a central one at the origin, corresponding to the flat band. These predictions are illustrated in figure 5, showing plots of the probability profiles $|\psi_n^{00}(t)|^2$ (left) and $|\psi_n^{01}(t)|^2$ (right) at time $t = 200$ against n (n serves as a proxy for the center-of-mass coordinate x_{cm}) for the $N = 3$ centipede launched at $t = 0$ at sites 0, 1 and 2, i.e., with a single non-zero amplitude $\psi_0^{00}(0) = 1$. The first profile exhibits a central peak, whereas the second one does not.

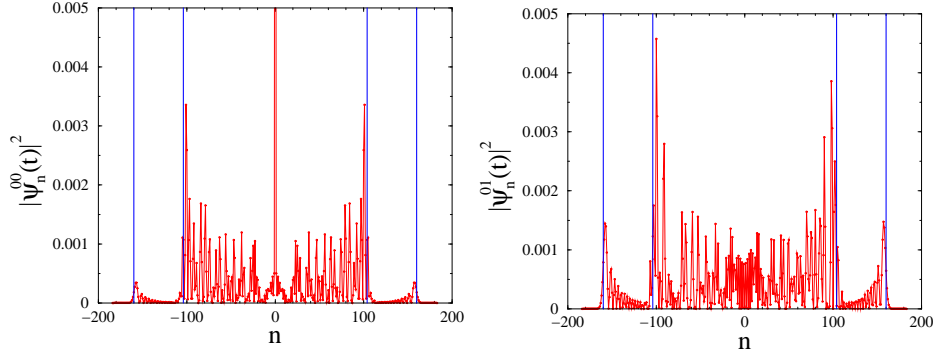


Figure 5. Two probability profiles at time $t = 200$ for the $N = 3$ centipede launched in its most compact state near the origin ($\psi_0^{00}(0) = 1$). Left: $|\psi_n^{00}(t)|^2$ exhibits a central peak (not to scale). Right: $|\psi_n^{01}(t)|^2$ does not. Vertical blue lines: nominal positions of the ballistic fronts at $\pm V^{(3)}t$ and $\pm V^{(3,1)}t$.

Equation (4.15) yields a cubic equation for the quasiparticle eigenvalues:

$$4\Lambda^3 - 5\Lambda \pm 2 \cos q = 0. \quad (5.13)$$

A comparison with (5.10) demonstrates that the correspondence (4.10) goes as follows for $N = 3$: the energies ω are twice as large as (some of) the quasiparticle eigenvalues Λ . Figure 6 shows the quasiparticle spectrum against q/π .

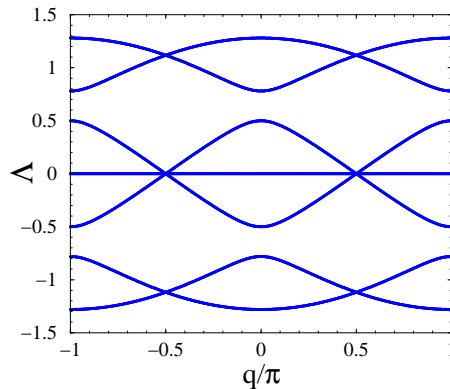


Figure 6. Quasiparticle spectrum of the $N = 3$ centipede against q/π .

- $N = 4$

The Hamiltonian reads

$$\mathcal{H} = \begin{pmatrix} 0 & 1 & 0 & 0 & e^{iq} & 0 & 0 & 0 \\ 1 & 0 & 1 & 0 & 0 & e^{iq} & 0 & 0 \\ 0 & 1 & 0 & 1 & 1 & 0 & e^{iq} & 0 \\ 0 & 0 & 1 & 0 & 0 & 1 & 0 & e^{iq} \\ e^{-iq} & 0 & 1 & 0 & 0 & 1 & 0 & 0 \\ 0 & e^{-iq} & 0 & 1 & 1 & 0 & 1 & 0 \\ 0 & 0 & e^{-iq} & 0 & 0 & 1 & 0 & 1 \\ 0 & 0 & 0 & e^{-iq} & 0 & 0 & 1 & 0 \end{pmatrix}. \quad (5.14)$$

The associated characteristic equation is

$$\omega^8 - 12\omega^6 + 4(8 - 3\cos q)\omega^4 - 24(1 - \cos q)\omega^2 + 4(1 - \cos q)^2 = 0. \quad (5.15)$$

Figure 7 shows plots of the energy spectrum (left) and of the group velocities (right) against q/π . The maximal velocities $\pm V^{(4)}$, with

$$V^{(4)} = \frac{1}{\sqrt{2}}, \quad (5.16)$$

are reached for $q = 0$. Figure 8 shows the quasiparticle spectrum against q/π . This is the first case where the correspondence (4.10) exhibits its generic nature, in the sense that it involves non-trivial linear combinations.

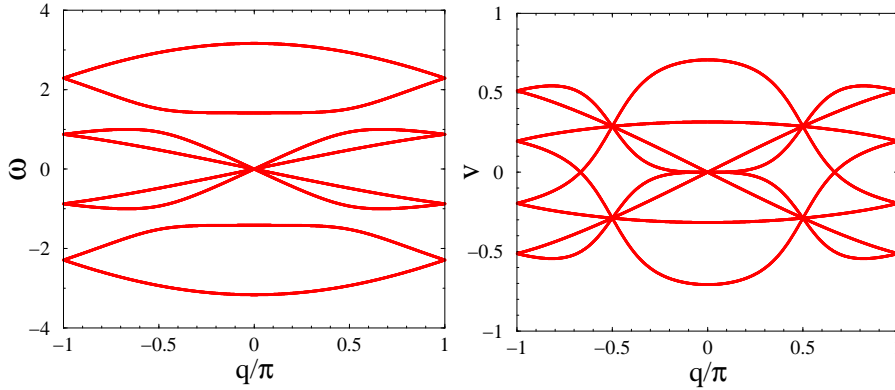


Figure 7. Left: energy spectrum of the $N = 4$ centipede against q/π . Right: associated group velocities.

- $N = 5$

We shall not write down the 16×16 Hamiltonian matrix \mathcal{H} explicitly. The associated characteristic equation is

$$\omega(\omega^5 - 7\omega^3 + 9\omega - 4\cos q)(A(\omega) - B(\omega)\cos q - 16\cos^2 q) = 0, \quad (5.17)$$

with

$$\begin{aligned} A(\omega) &= \omega^2(\omega^2 - 1)(\omega^2 - 13)(\omega^4 - 7\omega^2 + 9), \\ B(\omega) &= 4\omega(11\omega^4 - 28\omega^2 + 13). \end{aligned} \quad (5.18)$$

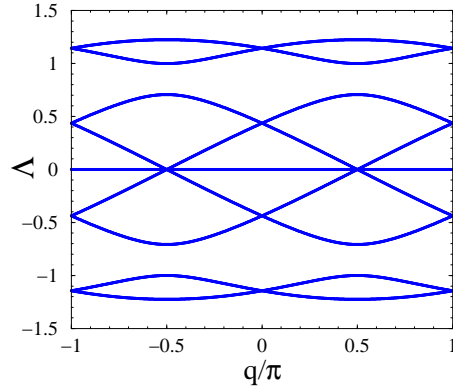


Figure 8. Quasiparticle spectrum of the $N = 4$ centipede against q/π .

Figure 9 shows plots of the energy spectrum (left) and of the group velocities (right) against q/π . The maximal velocities $\pm V^{(5)}$, with

$$V^{(5)} = \frac{26 + 14\sqrt{13}}{117} = 0.653\ 655\dots, \quad (5.19)$$

are respectively reached for $q = \mp\pi/2$. Figure 10 shows the quasiparticle spectrum against q/π .

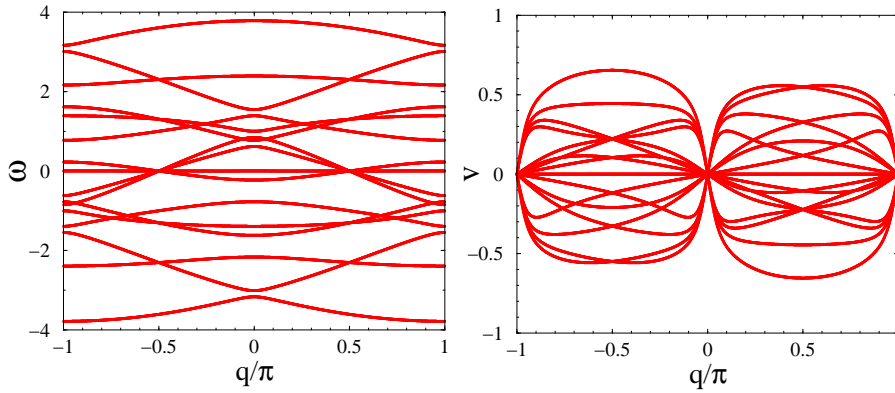


Figure 9. Left: energy spectrum of the $N = 5$ centipede against q/π . Right: associated group velocities.

The above results illustrate the general feature that the complexity of the energy spectrum of the centipede grows very fast as the fermion number N is increased. In particular the number of stationary values of the velocity satisfying (3.6), which are responsible for the occurrence of internal ballistic fronts, grows very rapidly with N . The quasiparticle spectrum however remains regular and simple, as the number of quasiparticle eigenvalues only grows linearly with N .

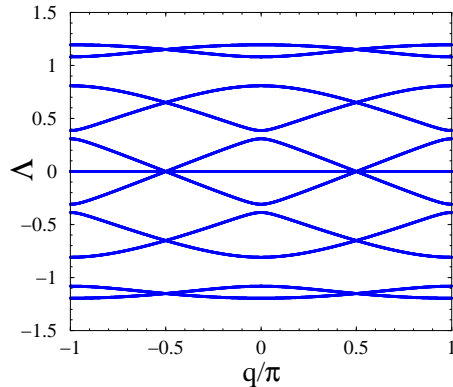


Figure 10. Quasiparticle spectrum of the $N = 5$ centipede against q/π .

6. Maximal spreading velocity for arbitrary N

The aim of this section is to obtain an exact expression of the maximal velocity $V^{(N)}$ of the centipede for an arbitrary fermion number N . This quantity, defined in (3.5), characterizes the ballistic spreading of the two extremal fronts of the wavefunction in the center-of-mass coordinate. We shall also derive the exact value of the limit $V^{(\infty)}$.

The explicit results given in section 5 for the first few values of N suggest the following pattern. The maximal velocity $V^{(N)}$ is reached for the values of the center-of-mass momentum q such that the right-hand side of the characteristic equations (4.14), (4.15) vanishes, i.e., $q = 0$ or $\pm\pi$ when N is even, whereas $q = \pm\pi/2$ when N is odd. In these situations, all the quasiparticle eigenvalues Λ_k are twofold degenerate. The simultaneous linear lifting of these degeneracies yields, by means of (4.10), the largest possible value of the group velocity.

Let us consider for definiteness the case where N is even, and set

$$\frac{\sin((N+1)p) - 3\sin((N-1)p)}{\sin p} = P_N(\Lambda), \quad (6.1)$$

with $\Lambda = \cos p$ (see (4.13), (A.9)). The function $P_N(\Lambda)$ thus defined is a polynomial with degree N , which can be expressed as a linear combination of two Chebyshev polynomials of the second kind [43]:

$$P_N(\Lambda) = U_N(\Lambda) - 3U_{N-2}(\Lambda). \quad (6.2)$$

The polynomials P_N obey the recursion

$$P_{N+1}(\Lambda) = 2\Lambda P_N(\Lambda) - P_{N-1}(\Lambda). \quad (6.3)$$

We have $P_0(\Lambda) = 4$, $P_1(\Lambda) = 2\Lambda$, $P_2(\Lambda) = 4(\Lambda^2 - 1)$, $P_3(\Lambda) = 2\Lambda(4\Lambda^2 - 5)$, and so on. The characteristic equation (4.14) can thus be recast as

$$P_N(\Lambda) = \pm 4 \sin q. \quad (6.4)$$

For $q = 0$ or $q = \pi$, the right-hand side vanishes. The doubly degenerate quasiparticle eigenvalues therefore coincide with the N roots Λ_k of the polynomial P_N . The lifting of these twofold degeneracies in the vicinity of $q = 0$ or $q = \pi$ is described by the slopes

$$\frac{d\Lambda_k}{dq} = \pm \frac{4}{P'_N(\Lambda_k)}. \quad (6.5)$$

Using (4.10), taking care about avoiding multiple counting, we obtain the expression

$$V^{(N)} = \sum_{k=1}^N \frac{4}{|P'_N(\Lambda_k)|} \quad (6.6)$$

for the maximal spreading velocity. The case where N is odd can be dealt with in a similar way and yields the same expression.

The general formula (6.6) allows us to recover (5.5), (5.11), (5.16), (5.19), i.e.,

$$\begin{aligned} V^{(2)} &= 1, & V^{(3)} &= \frac{4}{5} = 0.8, \\ V^{(4)} &= \frac{1}{\sqrt{2}} = 0.707\,106\dots, & V^{(5)} &= \frac{26 + 14\sqrt{13}}{117} = 0.653\,655\dots \end{aligned} \quad (6.7)$$

and to predict that

$$V^{(6)} = 0.620\,924\dots, \quad V^{(7)} = 0.600\,722\dots \quad (6.8)$$

are the largest roots of the polynomial equations $229V^4 - 78V^2 - 8V + 1 = 0$ and $79\,937V^3 - 49\,192V^2 - 3\,664V + 2\,624 = 0$, with respective degrees 4 and 3. More generally, the maximal velocity $V^{(N)}$ is an algebraic number whose degree d_N grows exponentially fast with N . Let us skip details and give the following result:

$$\begin{aligned} N = 2m \text{ even:} & & d_{2m} &= 2^{m-1}, \\ N = 2m + 1 \text{ odd:} & & d_{2m+1} &= \binom{m}{\text{Int}(m/2)}, \end{aligned} \quad (6.9)$$

where $\text{Int}(\cdot)$ denotes the integer part.

As the fermion number N increases, the velocities $V^{(N)}$ converge to a finite limit $V^{(\infty)}$, which can be obtained as follows. For $N \geq 3$, $N - 2$ roots Λ_k of the polynomial P_N obey $|\Lambda_k| < 1$. They correspond to real momenta p_k , such that

$$Np_k = k\pi + \theta_k \quad (k = 1, \dots, N - 2), \quad (6.10)$$

with $|\theta_k| \leq \pi/2$ and

$$\tan \theta_k = 2 \tan p_k. \quad (6.11)$$

The last two roots satisfy $|\Lambda| > 1$. They correspond to evanescent modes with complex momenta $p = i\zeta$ and $p = \pi + i\zeta$, such that $\Lambda = \pm \cosh \zeta$, with $\tanh(N\zeta) = 2 \tanh \zeta$. In the large- N limit, we have $\tanh \zeta \rightarrow 1/2$, and so $\zeta \rightarrow (\ln 3)/2$ (see (6.14)) and $\Lambda \rightarrow \pm 2/\sqrt{3}$.

By differentiating (6.1), using (6.10) and (6.11), we obtain the following estimate

$$|P'_N(\Lambda_k)| \approx \frac{2N}{\sin^2 p_k} \underbrace{(\cos \theta_k \cos p_k + 2 \sin \theta_k \sin p_k)}_{\sqrt{1 + 3 \sin^2 p_k}} \quad (6.12)$$

for large N and real momenta p_k . Finally, inserting the above expression into (6.6), and replacing the sum by an integral, we obtain

$$\begin{aligned} V^{(\infty)} &= \frac{4}{\pi} \int_0^{\pi/2} \frac{\sin^2 p \, dp}{\sqrt{1 + 3 \sin^2 p}} \\ &= \frac{2}{3\pi} \left(4\mathbf{E}\left(\frac{\sqrt{3}}{2}\right) - \mathbf{K}\left(\frac{\sqrt{3}}{2}\right) \right) = 0.570\,349\,449\dots, \end{aligned} \quad (6.13)$$

where \mathbf{E} and \mathbf{K} are the complete elliptic integrals [43].

Figure 11 illustrates the above results. The left panel shows a plot of $V^{(N)}$ against the fermion number N . The limit $V^{(\infty)}$ (see (6.13)) is shown as a blue line. The right panel shows a logarithmic plot of the difference $V^{(N)} - V^{(\infty)}$ against N . The data points are observed to become extremely close to the straight line with slope $-\zeta$, where

$$\zeta = \frac{\ln 3}{2} = 0.549\,306\dots \quad (6.14)$$

is the inverse penetration length of the evanescent modes. This clearly demonstrates that the velocities converge to their limit as $V^{(N)} - V^{(\infty)} \sim e^{-N\zeta}$, i.e., exponentially fast in N .

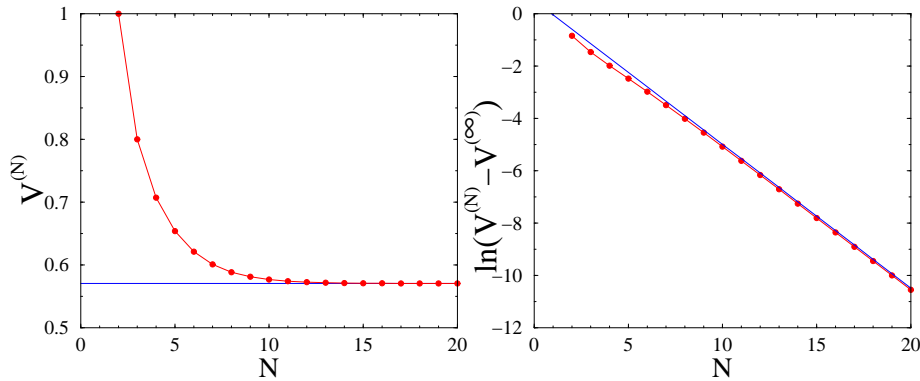


Figure 11. Left: plot of the extremal velocity $V^{(N)}$ against the fermion number N . Blue horizontal line: limit $V^{(\infty)}$ (see (6.13)). Right: logarithmic plot of difference $V^{(N)} - V^{(\infty)}$ against N . The blue straight line has slope $-\zeta$.

7. Discussion

We have investigated a quantum centipede made of N fermionic quantum walkers on the one-dimensional lattice interacting by the hard constraint that the distance between two successive fermions is either one or two lattice spacings. Besides the number N of fermions, the model is entirely parameter-free.

As in our previous work [24], the main emphasis has been put on the ballistic spreading of the wavefunction of the centipede in its center-of-mass coordinate. For a generic initial state located in the vicinity of the origin, the distribution profile of the velocity $v = n/t$ of the center of mass generically exhibits two extremal ballistic fronts at $\pm V^{(N)}$, as well as internal ballistic fronts, whose number grows rapidly with the number N of fermions.

The energy spectrum of the centipede and the corresponding velocity dispersion curve have been analyzed by direct means for the first few values of N , whereas some analytical results have been derived for arbitrary N by exploiting a mapping of the problem onto a free-fermion system. We have thus obtained the expression (6.6) of the maximal spreading velocity $V^{(N)}$, and the non-trivial result (6.13) for the limit $V^{(\infty)}$.

It is interesting to put the present findings in perspective with the results of [25] on the diffusive dynamics of N -legged molecules dubbed polypeds and spiders [44]. The

classical analogue of the present situation is that of symmetric molecular centipedes, whose diffusion coefficient is given (for all $N \geq 2$) by

$$D^{(N)} = \frac{1}{4(N-1)}. \quad (7.1)$$

There is a stark contrast between the fall-off of the diffusion coefficient $D^{(N)}$ for large N in the classical case and the convergence of the spreading velocity to a finite limit $V^{(\infty)}$ in the quantum case. This is yet another manifestation of the qualitatively different dynamical behavior of classical and quantum walkers.

Some of the properties of the quantum centipede depend on the parity of the fermion number N . The symmetries of the energy spectrum ensure the existence of a flat (i.e., non-dispersive) band when N is odd. As a consequence, the wavefunction of the centipede may exhibit a central peak near the origin for odd N . (This is illustrated in figure 5 for $N = 3$.) The occurrence of a central peak has been underlined in other types of quantum walks. For a single discrete-time walker equipped with a three-dimensional quantum coin, a localization phenomenon has been put forward, in the sense that a finite fraction of the probability stays forever in the vicinity of the particle's starting point [45, 46]. From a different perspective, parity effects are also known to affect transport properties of some quasi-one-dimensional systems. Disordered strips made of N coupled channels with purely off-diagonal disorder are known to exhibit conventional Anderson localization for even N , albeit unconventional localization properties for odd N , with a subexponential scaling of the conductance at the band center [47, 48, 49, 50].

In this work we have demonstrated that the simplest fermionic quantum centipede, with maximal separation $\ell = 2$ between neighboring particles, is tractable by analytical means. It would be interesting to investigate fermionic or bosonic quantum centipedes with larger maximal separations as well. Classical centipedes with $\ell \geq 3$ however lead to extremely complicated results, so that the general case seems intractable [25]. Another variant that has been studied in the classical case is a centipede whose total length never exceeds some given length L [25]. Its quantum analogue also appears to be interesting. Finally, it might also be worth considering bound states of N quantum walkers, either fermionic or bosonic, on higher-dimensional lattices with various kinds of hard-bound constraints.

Appendix A. Derivation of the characteristic equations (4.14), (4.15)

In this appendix we provide a detailed characterization of the quasiparticle operators defined in (4.11) and a derivation of the characteristic equations (4.14), (4.15).

Our starting point is the quadratic identity

$$[\tau_j^\mu \tau_{j+1}^\nu, \tau_k^\lambda] = 2(\delta_{j+1,k} \delta^{\nu\lambda} \tau_j^\mu - \delta_{jk} \delta^{\mu\lambda} \tau_{j+1}^\nu), \quad (\text{A.1})$$

where $\mu, \nu, \lambda = x, y$, that follows from the Clifford algebra (4.6). We can then write explicitly the commutation relation $[\mathcal{H}_{\text{long}}, a_k] = -2\Lambda_k a_k$ (see (4.12)) as follows

$$\begin{aligned} & i \cos q (x_1 \tau_0^y - y_0 \tau_1^x) + i \sin q (-y_0 \tau_1^y + y_1 \tau_0^y) \\ & + \frac{i}{2} \sum_{j=1}^{N-2} (x_{j+1} \tau_j^y + x_j \tau_{j+1}^y - y_j \tau_{j+1}^x - y_{j+1} \tau_j^x) \\ & + i (x_N \tau_{N-1}^y - y_{N-1} \tau_N^x) = \Lambda \sum_{j=0}^N (x_j \tau_j^x + y_j \tau_j^y). \end{aligned} \quad (\text{A.2})$$

(The subscript $k = 0, \dots, N$ has been omitted for ease of reading.) After identifying the coefficients of each $\tau_j^{x,y}$, we obtain the following system of linear equations for the coefficients x_j and y_j :

For $j = 0$:

$$x_0 = 0, \quad -i\Lambda y_0 = x_1 \cos q + y_1 \sin q. \quad (\text{A.3})$$

For $j = 1$:

$$2i\Lambda x_1 = 2y_0 \cos q + y_2, \quad -2i\Lambda y_1 = x_2 - 2y_0 \sin q. \quad (\text{A.4})$$

For $j = 2, \dots, N - 2$:

$$2i\Lambda x_j = y_{j-1} + y_{j+1}, \quad -2i\Lambda y_j = x_{j-1} + x_{j+1}. \quad (\text{A.5})$$

For $j = N - 1$:

$$2i\Lambda x_{N-1} = y_{N-2}, \quad -2i\Lambda y_{N-1} = x_{N-2} + 2x_N. \quad (\text{A.6})$$

For $j = N$:

$$i\Lambda x_N = y_{N-1}, \quad y_N = 0. \quad (\text{A.7})$$

The above equations can be interpreted as an eigenvalue problem for the vector $(x_0, y_0, x_1, y_1, \dots, x_N, y_N)$ of length $2(N + 1)$. The quasiparticle eigenvalues Λ are obtained as follows. The bulk equations (A.5) yield the recursion

$$4\Lambda^2 x_j = x_{j-2} + 2x_j + x_{j+2} \quad (j = 2, \dots, N - 2). \quad (\text{A.8})$$

The corresponding characteristic equation is bi-quadratic: $4\Lambda^2 = r^{-2} + 2 + r^2 = (r^{-1} + r)^2$. The four values $r = \pm e^{\pm ip}$ lead to the dispersion relation

$$\Lambda = \cos p. \quad (\text{A.9})$$

Using (A.5) and (A.9), the corresponding eigenvectors read

$$\begin{aligned} x_j &= Ae^{ijp} + Be^{-ijp} + (-1)^j (Ce^{ijp} + De^{-ijp}), \\ -iy_j &= Ae^{ijp} + Be^{-ijp} - (-1)^j (Ce^{ijp} + De^{-ijp}). \end{aligned} \quad (\text{A.10})$$

The values of p are yet to be determined by the boundary conditions. First, using (A.3) and (A.7), we substitute y_0 and x_N in (A.4) and (A.6) to obtain

$$\begin{aligned} 2\Lambda^2 x_1 &= (1 + \cos 2q)x_1 + \sin 2q y_1 - i\Lambda y_2, \\ 2\Lambda^2 y_1 &= \sin 2q x_1 + (1 - \cos 2q)y_1 + i\Lambda x_2, \\ 2i\Lambda x_{N-1} &= y_{N-2}, \\ 2\Lambda^2 y_{N-1} &= i\Lambda x_{N-2} + 2y_{N-1}. \end{aligned} \quad (\text{A.11})$$

Then, imposing that the generic forms (A.10) remain valid for $j = 1$ and $j = N - 1$, (A.11) yields

$$\begin{aligned} e^{2iq}(e^{ip}A + e^{-ip}B) - i \sin p (C - D) &= 0, \\ i \sin p (A - B) - e^{-2iq}(e^{ip}C + e^{-ip}D) &= 0, \\ e^{iNp}A + e^{-iNp}B - (-1)^N (e^{iNp}C + e^{-iNp}D) &= 0, \\ e^{iNp}(e^{ip} - 3e^{-ip})A + e^{-iNp}(e^{-ip} - 3e^{ip})B \\ + (-1)^N (e^{iNp}(e^{ip} - 3e^{-ip})C + e^{-iNp}(e^{-ip} - 3e^{ip})D) &= 0. \end{aligned} \quad (\text{A.12})$$

Expressing that the 4×4 determinant of this system vanishes, we get

$$\begin{aligned} \cos(2(N + 1)p) - 6 \cos(2Np) + 9 \cos(2(N - 1)p) \\ = 2(1 + \cos 2p) + 8(-1)^N \cos 2q (1 - \cos 2p). \end{aligned} \quad (\text{A.13})$$

The characteristic equation thus obtained is a polynomial equation with degree $N + 1$ in the variable $\cos 2p = 2\Lambda^2 - 1$. The value $p = 0$ is however not allowed. The eigenvectors constructed as above indeed vanish identically for $p = 0$. We are thus left with N pairs of opposite quasiparticle eigenvalues $\pm\Lambda_k$. This spectrum is to be completed by $\Lambda = 0$ with multiplicity two. For $e^{ip} = \pm i$ the system (A.12) indeed always admits the solution $A = B = C = D$, irrespective of q . This elementary non-dispersive solution had been discarded in the algebra leading to (A.13).

Inserting the above quasiparticle spectrum into (4.10) yields the 2^{N+1} (possibly degenerate) eigenvalues ω_{long} of $\mathcal{H}_{\text{long}}$. A quarter of them, corresponding to the sector $(+1, +1)$ of the boundary operators S_0^x and S_N^x , coincide with the 2^{N-1} (again possibly degenerate) eigenvalues ω of \mathcal{H} .

Finally, the characteristic equation (A.13) can be further simplified to (4.14) and (4.15), by dealing separately with even and odd values of N .

References

- [1] Aharonov Y, Davidovich L and Zagury N 1993 Quantum random walks *Phys. Rev. A* **48** 1687
- [2] Farhi E and Gutmann S 1998 Quantum computation and decision trees *Phys. Rev. A* **58** 915
- [3] Childs A M 2009 Universal computation by quantum walk *Phys. Rev. Lett.* **102** 180501
- [4] Kempe J 2003 Quantum random walks – an introductory overview *Contemp. Phys.* **44** 307
- [5] Ambainis A 2003 Quantum walks and their algorithmic applications *Int. J. Quantum Inf.* **1** 507
- [6] Venegas-Andraca S E 2012 Quantum walks: a comprehensive review *Quantum Inf. Process.* **11** 1015
- [7] Ryan C A, Laforest M, Boileau J C and Laflamme R 2005 Experimental implementation of a discrete-time quantum random walk on an NMR quantum-information processor *Phys. Rev. A* **72** 062317
- [8] Schmitz H, Matjeschek R, Schneider C, Glueckert J, Enderlein M, Huber T and Schaetz T 2009 Quantum walk of a trapped ion in phase space *Phys. Rev. Lett.* **103** 090504
- [9] Zähringer F, Kirchmair G, Gerritsma R, Solano E, Blatt R and Roos C F 2010 Realization of a quantum walk with one and two trapped ions *Phys. Rev. Lett.* **104** 100503
- [10] Karski M, Förster L, Choi J M, Steffen A, Alt W, Meschede D and Widera A 2009 Quantum walk in position space with single optically trapped atoms *Science* **325** 174
- [11] Schreiber A, Cassemiro K N, Potoček V, Gábris A, Mosley P J, Andersson E, Jex I and Silberhorn C 2010 Photons walking the line: A quantum walk with adjustable coin operations *Phys. Rev. Lett.* **104** 050502
- [12] Knight P L, Roldán E and Sipe J E 2003 Quantum walk on the line as an interference phenomenon *Phys. Rev. A* **68** 020301(R)
- [13] Perets H B, Lahini Y, Pozzi F, Sorel M, Morandotti R and Silberberg Y 2008 Realization of quantum walks with negligible decoherence in waveguide lattices *Phys. Rev. Lett.* **100** 170506
- [14] Hillery M 2010 Quantum walks through a waveguide maze *Science* **329** 1477
- [15] Peruzzo A, Lobino M, Matthews J C F, Matsuda N, Politi A, Poulios K, Zhou X Q, Lahini Y, Ismail N, Wörhoff K, Bromberg Y, Silberberg Y, Thompson M G and O'Brien J L 2010 Quantum walk of correlated photons *Science* **329** 1500
- [16] Lahini Y, Bromberg Y, Christodoulides D N and Silberberg Y 2010 Quantum correlations in two-particle Anderson localization *Phys. Rev. Lett.* **105** 163905
- [17] Sansoni L, Sciarrino F, Vallone G, Mataloni P, Crespi A, Ramponi R and Osellame R 2012 Two-particle bosonic-fermionic quantum walk via integrated photonics *Phys. Rev. Lett.* **108** 010502
- [18] Omar Y, Paunkovic N, Sheridan L and Bose S 2006 Quantum walk on a line with two entangled particles *Phys. Rev. A* **74** 042304
- [19] Gamble J K, Friesen M, Zhou D, Joynt R and Coppersmith S N 2010 Two-particle quantum walks applied to the graph isomorphism problem *Phys. Rev. A* **81** 052313
- [20] Štefaňák M, Barnett S M, Kollár B, Kiss T and Jex I 2011 Directional correlations in quantum walks with two particles *New J. Phys.* **13** 033029
- [21] Chandrashekar C M and Busch T 2012 Quantum walk on distinguishable non-interacting many-particles and indistinguishable two-particle *Quantum Inf. Process.* **11** 1287
- [22] Qin X, Ke Y, Guan X W, Li Z, Andrei N and Lee C 2014 Statistics-dependent quantum co-

- walking of two particles in one-dimensional lattices with nearest-neighbor interaction *Phys. Rev. A* **90** 062301
- [23] de Toro Arias S and Luck J M 1998 Anomalous dynamical scaling and multifractality in the one-dimensional Anderson model *J. Phys. A: Math. Gen.* **31** 7699
- [24] Krapivsky P L, Luck J M and Mallick K 2015 Interacting quantum walkers: Two-body bosonic and fermionic bound states *J. Phys. A: Math. Theor.* **48** 475301
- [25] Antal T, Krapivsky P L and Mallick K 2007 Molecular spiders in one dimension *J. Stat. Mech.* **2007** P08027
- [26] Baraviera A, Franco T and Neumann A 2015 Hydrodynamic limit of quantum random walks in *From Particle Systems to Partial Differential Equations II* Springer Proceedings in Mathematics & Statistics **129** [arXiv:1309.1146]
- [27] Grimmett G, Janson S and Scudo P F 2004 Weak limits of quantum random walks *Phys. Rev. E* **69** 026119
- [28] Gottlieb A D 2005 Convergence of continuous-time quantum walks on the line *Phys. Rev. E* **72** 047102
- [29] Konno N 2005 Limit theorem for continuous-time quantum walk on the line *Phys. Rev. E* **72** 026113
- [30] Strauch F W 2006 Connecting the discrete- and the continuous-time quantum walk *Phys. Rev. A* **74** 030301(R)
- [31] Mülken O, Pernice V and Blumen A 2008 Universal behavior of quantum walks with long-range steps *Phys. Rev. E* **77** 021117
- [32] Mülken O and Blumen A 2011 Continuous-time quantum walks: Models for coherent transport on complex networks *Phys. Rep.* **502** 37
- [33] Xu X P 2008 Continuous-time quantum walks on one-dimensional regular networks *Phys. Rev. E* **77** 061127
- [34] Xu X P 2009 Coherent exciton transport and trapping on long-range interacting cycles *Phys. Rev. E* **79** 011117
- [35] Geim A K and Novoselov K S 2007 The rise of graphene *Nature Materials* **6** 183
- [36] Castro-Neto A H, Guinea F, Peres N M R, Novoselov K S and Geim A K 2009 The electronic properties of graphene *Rev. Mod. Phys.* **81** 109
- [37] Krapivsky P L, Redner S and Ben-Naim E 2010 *A Kinetic View of Statistical Physics* (Cambridge: Cambridge University Press)
- [38] Nepomechie R I 2001 Bethe Ansatz solution of the open XX spin chain with non-diagonal boundary terms *J. Phys. A: Math. Gen.* **34** 9993
- [39] Šamaj L and Bajnok J 2013 *Introduction to the Statistical Physics of Integrable Many-body Systems* (Cambridge: Cambridge University Press)
- [40] Lieb E, Schultz T and Mattis D 1961 Two soluble models of an antiferromagnetic chain *Ann. Phys.* **16** 407
- [41] Hinrichsen H, Krebs K and Peschel I 1996 Solution of a one-dimensional diffusion-reaction model with spatial asymmetry *Z. Phys. B* **100** 105
- [42] Bilstein U and Wehefritz B 1999 The XX-model with boundaries: Part I. Diagonalisation of the finite chain *J. Phys. A: Math. Gen.* **32** 191
- [43] Gradshteyn I S and Ryzhik I M 1965 *Table of Integrals, Series, and Products* (New York: Academic)
- [44] Pei R, Taylor S K, Stefanović D, Rudchenko S, Mitchell T E and Stojanovic M N 2006 Behavior of polycatalytic assemblies in a substrate-displaying matrix *J. Am. Chem. Soc.* **128** 12693
- [45] Inui N, Konno N and Segawa E 2005 One-dimensional three-state quantum walk *Phys. Rev. E* **72** 056112
- [46] Štefaňák M, Bezdekova I and Jex I 2014 Limit distributions of three-state quantum walks: The role of coin eigenstates *Phys. Rev. A* **90** 012342
- [47] Brouwer P W, Mudry C, Simons B D and Altland A 1998 Delocalization in coupled one-dimensional chains *Phys. Rev. Lett.* **81** 862
- [48] Mudry C, Brouwer P W and Furusaki A 1999 Random magnetic flux problem in a quantum wire *Phys. Rev. B* **59** 13221
- [49] Mudry C, Brouwer P W and Furusaki A 1999 Crossover from the chiral to the standard universality classes in the conductance of a quantum wire with random hopping only *Phys. Rev. B* **62** 8249
- [50] Brouwer P W, Mudry C and Furusaki A 2000 Nonuniversality in quantum wires with off-diagonal disorder: a geometric point of view *Nucl. Phys. B* **565** 653